PCCP

PAPER

View Article Online
View Journal | View Issue

Cite this: *Phys. Chem. Chem. Phys.*, 2023, **25**, 23923

Stepwise hydration of $[CH_3COOMg]^+$ studied by cold ion trap infrared spectroscopy: insights into interactions in the magnesium channel selection filters†

Hikaru Takayanagi,‡[ab] Jean-Xavier Bardaud, §‡[c] Keisuke Hirata,[ad] Valérie Brenner, ¶[c] Eric Gloaguen, §*[c] Shun-ichi Ishiuchi *[ad] and Masaaki Fujii *[abe]

Received 3rd March 2023,
Accepted 16th August 2023

DOI: 10.1039/d3cp00992k

rsc.li/pccp

The magnesium channel controls Mg^{2+} concentration in the cell and plays an indispensable role in biological functions. The crystal structure of the Magnesium Transport E channel suggested that Mg^{2+} hydrated by 6 water molecules is transported through a selection filter consisting of COO^- groups on two Asp residues. This Mg^{2+} motion implies successive pairing with $^-$OOC-R and dissociation mediated by water molecules. For another divalent ion, however, it is known that $RCOO^-\cdots Ca^{2+}$ cannot be separated even with 12 water molecules. From this discrepancy, we probe the structure of $Mg^{2+}(CH_3COO^-)(H_2O)_{4-17}$ clusters by measuring the infrared spectra and monitoring the vibrational frequencies of COO^- with the help of quantum chemistry calculations. The hydration by $(H_2O)_6$ is not enough to induce ion separation, and partially-separated or separated pairs are formed from 10 water molecules at least. These results suggest that the ion separation between Mg^{2+} and carboxylate ions in the selection-filter of the MgtE channel not only results from water molecules in their first hydration shell, but also from additional factors including water molecules and protein groups in the second solvation shell of Mg^{2+}.

1. Introduction

Ion channels are membrane proteins that selectively permeate specific ions and play an important role in biological systems.[1–4] The mechanism of ion selectivity depends on the type of ion channel, but the simplest understanding is a competition between the ion affinity of the channel and the solvation of the ion. For example, in the case of potassium, the selective filter motif at the channel opening has several carbonyl groups, which are responsible for ion selection.[1,2] This ion selection is achieved because the interaction energy of the carbonyl group with the potassium ion is slightly more favorable than the hydration energy of the potassium ion, whereas the sodium ion cannot enter the ion channel because its hydration energy is more favorable. Further detailed understanding at the molecular level has been gained by using X-ray diffraction,[1,2] 2D infrared spectroscopy,[5] molecular dynamics simulations,[6–8] and bottom-up approaches in which the interactions between parts of the selection filter and metal ions are studied by cold ion trap laser spectroscopy.[9–12]

The magnesium channel is one of the ion channels that controls Mg^{2+} concentration in the cell.[13–17] The magnesium ion is the most popular divalent ion in biological cells and is essential for life because of its role in biological functions, such as RNA and protein formation, catalysis by enzymes and so on.[18] Recently, the crystal structure of Magnesium Transport E (MgtE), a type of Mg^{2+} channel, has been revealed by Nureki's group[19–21] raising questions about Mg^{2+} transport mechanism and selectivity still under investigation.[22] According to this report, the selection filter responsible for selectivity consists of two COO^- groups on two Asp residues. This anionic moiety

[a] *Laboratory for Chemistry and Life Science, Institute of Innovative Research, Tokyo Institute of Technology, 4259 Nagatsuta-cho, Midori-ku, Yokohama, 226-8503, Japan. E-mail: ishiuchi.s.aa@m.titech.ac.jp, mfujii@res.titech.ac.jp*
[b] *School of Life Science and Technology, Tokyo Institute of Technology, 4259 Nagatsuta-cho, Midori-ku, Yokohama, Kanagawa, 226-8503, Japan*
[c] *LIDYL, CEA, CNRS, Université Paris Saclay, CEA Saclay, Bât 522, Gif-sur-Yvette 91191, France. E-mail: eric.gloaguen@cnrs.fr*
[d] *Department of Chemistry, School of Science, Tokyo Institute of Technology, 2-12-1 Ookayama, Meguro-ku, Tokyo 152-8550, Japan*
[e] *IRFI/IPWR, Institute of Innovative Research, Tokyo Institute of Technology, 4259 Nagatsuta-cho, Midori-ku, Yokohama, 226-8503, Japan*

† Electronic supplementary information (ESI) available: Experimental Methods; Theoretical methods; Structures. See DOI: https://doi.org/10.1039/d3cp00992k

‡ Contributed equally.

§ Present address: Université Paris-Saclay, CNRS, ISMO, 91400 Orsay, France.
¶ Present address: Direction de la recherche fondamentale, Commissariat à l'énergie atomique et aux énergies alternatives, CEA Saclay – 91191 Gif-sur-Yvette, Bât 530 – p 319B, France.

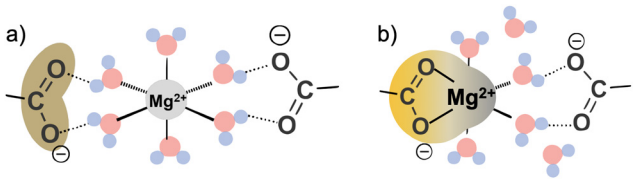

Fig. 1 (a) $Mg^{2+}(H_2O)_6$ transportation through the $-COO^-$ selection filter and (b) full contact ion pair formation with 6 H_2O. The former corresponds to separated ion pair of $R-COO^-Mg^{2+}$ by hydration (Solvent separated Ion Pair in solution chemistry).

does not bind directly to Mg^{2+}, but binds to the water molecule-clad Mg^{2+} in an octahedral arrangement, thus exerting ion selectivity. In the crystal structure analysis, 13 water molecules are found in the channel, but only 6 in the vicinity of Mg^{2+}, which is interpreted as the transportation of Mg^{2+} hydrated by 6 water molecules, $Mg^{2+}(H_2O)_6$, *i.e.* corresponding to a complete first hydration shell for this ion. The transportation of Mg^{2+} hydrated by its first solvation shell seems to be preferred over the transportation of the isolated divalent ion (see Fig. 1a).[21] Indeed, the hydration shell appears necessary to avoid the strong interactions that can occur between the divalent ion and the channel,[10] and contributes to smooth transport.

Here, we would like to raise a new viewpoint on Mg^{2+} transportation in MgtE. With a small number of water molecules, Mg^{2+} and $R-COO^-$ can bind to form a full contact ion pair because of their strong electrostatic interaction (see Fig. 1b), but such a contact has not been observed in the crystal structure.[21] Instead, the transportation of $Mg^{2+}(H_2O)_6$ through the $-COO^-$ selection filter involves two separated ion pairs between Mg^{2+} and two opposite carboxylate groups where ions are separated by hydration (see Fig. 1a). One may think that the second $-COO^-$ may help to keep such a centred position of Mg^{2+}, however the presence of a two charge system never guarantees such an equilibrium at the centre of the two charges like Fig. 1a. In general, such a two-charge centre system may also lead to a double minimum potential, which is the reason why *e.g.* a lithium cation prefers to bind to one of the oxygen of the carboxylate group instead of making two equal interactions with the oxygen atoms (bidentate binding) in crystals[23] as well as in solution.[24] Such a double minimum potential would put the Mg^{2+} cation in one side, like in Fig. 1b.

Such solvent induced ion pair separation has been extensively studied by gas-phase laser spectroscopy and *ab initio* calculations on solvated clusters, such as Li^+I^- and Cs^+I^-,[25] $Mg^{2+}HO^-$,[26] Na^+AcO^-,[27] Na^+Cl^-,[28,29] $Mg^{2+}RCOO^-$,[30] $Ca^{2+}RCOO^-$,[30–32] $Ba^{2+}AcO^-$[32] and $LiCl_2^-$.[33] These studies show that 5 or 6 solvent molecules are barely enough to separate pairs made of monovalent ions. For divalent ions, however, no separation has been observed for the cluster size investigated. Recent results on $RCOO^-\cdots Ca^{2+}$ ion pairs[31] demonstrated that even 12 water molecules are not able to separate these ions. Although the chemical properties of Ca^{2+} and Mg^{2+} are not the same,[34] both are divalent ions capable of binding strongly to $RCOO^-$. Then, it is legitimate to wonder whether six water molecules are intrinsically enough to separate $-COO^-$ and Mg^{2+} or not. If not, additional factors must help to keep these ions separated in the channel as observed by XRD.[21]

In order to solve the discrepancy between $Mg^{2+}(H_2O)_6$ transport in MgtE and the accumulated knowledge of ion pair separation by solvent molecules, we have applied cold ion trap spectroscopy[35–39] to hydrated $Mg^{2+}(CH_3COO^-)$ clusters, which serve as minimum model systems of the selection filter in MgtE. Infrared spectra can sensitively probe the coordination and H-bonds in hydrated $Mg^{2+}(CH_3COO^-)$ clusters. With the help of quantum chemistry calculations, we can discuss whether a solvent-separated ion pair state which corresponds to the $Mg^{2+}(H_2O)_6$ transport, is formed from $Mg^{2+}(CH_3COO^-)$ by hydration of six water molecules or not.

2. Methods

The experimental procedure is described in a previous article except for an additional quadruple ion mass spectrometer (Q-MS) before the first ion trap, which generate hydrated clusters (Fig. S1, ESI†). $[CH_3COOMg]^+$ is introduced into vacuum from electrospray (ESI) source (2.5×10^{-4} M in methanol solution). The ions are collected by ion funnel and introduced into the first Q-MS. The mass-selected ions are trapped by the first clustering ion trap[40,41] at 130 K, in which water vapor and He buffer gas are filled. The hydrated ions, $(CH_3COOMg)^+\cdot(H_2O)_n$ are further mass-selected by the second Q-MS, and then are introduced into the cryogenic quadruple ion trap (QIT) at 4 K. The QIT was cooled to 4 K by a closed cycle He refrigerator. A buffer gas (He/H_2 (20%)) was injected into the QIT *via* a pulsed nozzle, and H_2 were able to attach the hydrated complex ions. Then, a tunable IR laser (OPO/OPA: LaserVision) was introduced into the ion trap and scanned over the range of CO stretching vibrational range (1300 to 1800 cm^{-1}). When the frequency of the IR laser is resonant to vibrational levels of H_2-tagged clusters, H_2 is dissociated. Then, the infrared photodissociation (IRPD) spectra, which correspond to the IR absorption spectra, can be measured by monitoring the H_2-lossed ion intensity as a function of the IR laser wavenumber (H_2-tagging method). Here, the fragment ions were measured by time-of-flight mass spectrometer (TOF-MS), and ion signal is digitized and integrated in PC *via* a digital oscilloscope. Following the investigation of $[CH_3COOMg]^+(H_2O)_n$ (n = 1–5) by DePalma *et al.*,[30] we measured the infrared spectra of $[CH_3COOMg]^+(H_2O)_n$ from n = 4 to 17, and discussed the change of ion pair solvation state by stepwise hydration with the help of theoretical calculations (see ESI†).

We performed two steps of theoretical calculations. The first calculations are simpler one to estimate the vibrational signatures that indicate the solvation condition of Mg^{2+} from CH_3COO^-, such as full-contact ion pair state (bidentate ion pair), dissociated state (solvent-shared ion pair) and semi-dissociated state (monodentate ion pair) structures. For this purpose, IR spectra of $(CH_3COOMg)^+\cdot(H_2O)_6$ are calculated by density functional theory (DFT) calculations at CAM-B3LYP-D3/6-311+G(d,p)[42–45] level by using Gaussian 16. Optimized

structures of three different bonding states are reported for $(CH_3COOMg)^+\cdot(H_2O)_6$ by the DFT calculations without dispersion correction and the theoretical spectra are not shown.[46] We build the three initial structures according to the previous work, and the geometries are optimized by the dispersion corrected DFT calculations. The calculations give several conformations for a single ionic condition (such as the dissociated state). The conformational difference is relatively the minor part in relation to the ionic condition, so that we obtained the theoretical IR spectra for three typical ionic conditions. The obtained harmonic vibrational frequencies were scaled by 0.985. The performance and limitation of this well-known approach used to compare experimental and theoretical frequencies can be found *e.g.* in Section 5 of ref. 47 and ref. therein.

The RI-B97-D3/dhf-TZVPP[42,48,49] level of calculation (TURBOMOLE package[50]) was used for quantitative comparison with experimental results obtained on $(CH_3COOMg)^+\cdot(H_2O)_n$ clusters for n = 10 and 14. The potential energy surface of these systems being too complex for an exhaustive structural exploration, only a sample of selected structures was considered for geometry optimization (see ESI† for detail). These initial structures were either built from educated guesses, or randomly chosen among previously optimized structures of analogue $[CH_3COONa](H_2O)_n$ ($n > 14$) clusters[24,51] by replacing Na^+ by Mg^{2+} and removing water molecules in excess. These initial structures were optimized by the DFT calculations and vibrational frequencies were calculated at the same level. Optimized structures were sorted according to the type of ion pair formed, *i.e.* either bidentate or monodentate contact ion pairs, or solvent-shared ion pairs, thus defining three families of structures for each cluster size. Their Gibbs energy are reported on Fig. S2 (ESI†) and frequencies and intensities are reported on Tables S1–S6 (ESI†). Then, an averaged spectrum for each family and each size was obtained by averaging energy-weighted frequencies and intensities of each individual structures according to a procedure detailed in Section S4 (ESI†). Finally, an arbitrary spectral width of 6 cm^{-1} was chosen in order to model each vibrational transition by a Gaussian function, and present their sums as full theoretical spectra for comparison with the experimental ones.

3. Results and discussion

Prior to spectroscopic measurements, DFT calculations (CAM-B3LYP-D3/6-311+G(d,p)) were performed on $[CH_3COOMg]^+\cdot(H_2O)_6$ to estimate the vibrational signatures of each type of ion pair (see Section S3 in ESI†). We optimized three typical structures of $[CH_3COOMg]^+\cdot(H_2O)_6$ in which COO– binds to Mg^{2+} either as a full-contact ion pair state (bidentate), a partially-separated state (monodentate), or a separated state (no coordination). The obtained theoretical spectra and structures are shown in Fig. 2. In the full-contact ion pair state, from the low wavenumber side, each band is assigned to δ^{CH}, ν_s^{coo-}, ν_{as}^{coo-} and δ^{HOH}. However, in separated and partial-dissociated

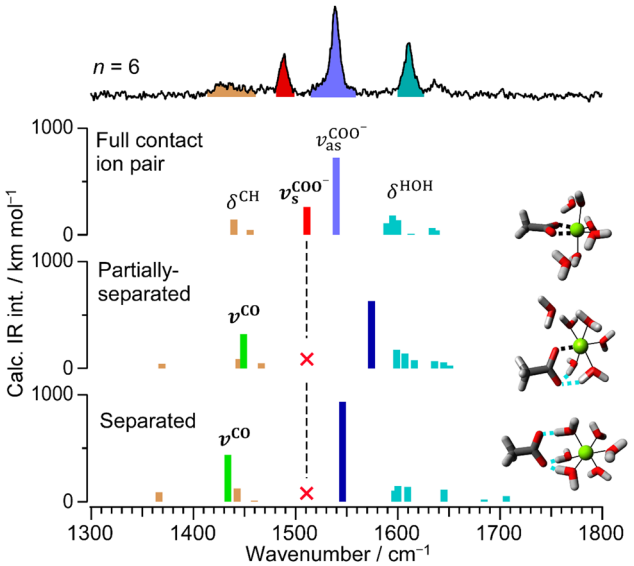

Fig. 2 Calculated stick spectra of $[CH_3COOMg]^+\cdot(H_2O)_6$ for full-contact, partially-separated and separated ion pairs with the IRPD spectrum of $[CH_3COOMg]^+\cdot(H_2O)_6$.

states, ν_s^{coo-} and ν_{as}^{coo-} are no more observed and replaced with two decoupled ν^{co} modes, one of which being observed at 1430–1450 cm^{-1} instead of ~1510 cm^{-1} for ν_{as}^{coo-} in the full contact ion pair. Thus, a transition at 1510 cm^{-1} is a signature specific to bidentate ion pairs. The intensities of the ν^{co} modes at 1430–1450 cm^{-1} are enhanced significantly in the separated state and mildly in the partially-separated, and can thus be used to monitor the formation of these states. Similarly, the enhancement of ν^{co} near 1550 cm^{-1} can be an indicator of the separated state, although it may overlap with ν_{as}^{coo-} in the case of a mixture of different types of structures. From these expectations, we measured the infrared spectra of $[CH_3COOMg]^+\cdot(H_2O)_n$.

Fig. 3 shows the infrared spectra of $[CH_3COOMg]^+\cdot(H_2O)_n$ (n = 4–17). The spectra of n = 4 and 5 reproduce those of a previous report,[30] and the spectral changes from n = 4 to n = 9 are relatively minor. These spectra can be assigned to the full-contact ion pair state according to our calculations. They are indeed consistent with the corresponding theoretical spectrum for n = 6 in Fig. 2, where the observed vibrational bands are assigned to δ^{CH}, ν_s^{coo-}, ν_{as}^{coo-} and δ^{HOH} as indicated in the figure. Among the minor changes in this series, the general blue shift of ν_{as}^{coo-} results from the motion away from the cation in full contact, induced by hydration by an increasing number of water molecules as already observed in the case of Ca^{2+}.[31,32] The blue shift of δ^{HOH} between n = 6 and n = 9 suggests the formation of the second hydrated shell from the analogy to the infrared spectra of $[CD_3CD_2COOCa]^+(H_2O)_n$ ($n \leq 12$),[31] in which the ion pair $COO^-\cdots Ca^{2+}$ keeps the full contact structure. From these infrared spectra, we conclude that Mg^{2+} is in full contact with COO^- in $[CH_3COOMg]^+(H_2O)_6$, and thus that the solvent-separated ion pair (see Fig. 1a), which is involved in the transportation of $Mg^{2+}(H_2O)_6$ in MgtE in solution, is intrinsically not stable enough to be formed with only six, or

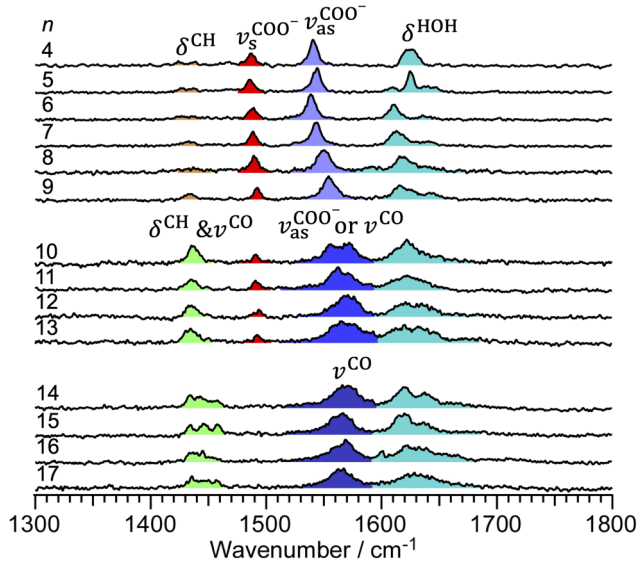

Fig. 3 Infrared photodissociation spectra of $[CH_3COOMg]^+(H_2O)_n$ (n = 4–17).

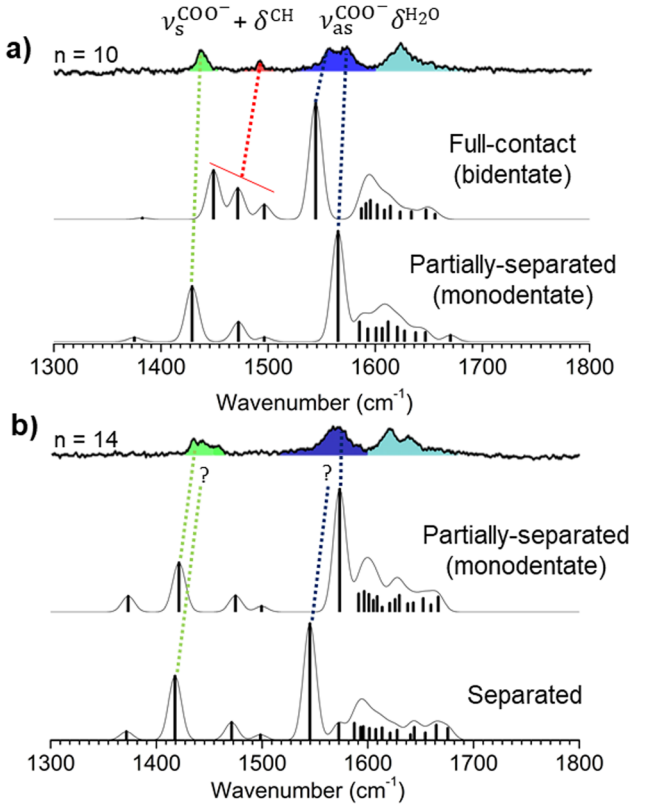

Fig. 4 RI-B97-D3/dhf-TZVPP mode-dependent scaled harmonic vibrational spectra compared to IRPD spectra for n = 10 (a) and n = 14 (b)

even nine water molecules. In contrast, the XRD study[21] clearly shows the presence of the $Mg^{2+}(H_2O)_6$ of octahedral hydration structure separated from COO^-. Then, the formation of the separated $Mg^{2+}(H_2O)_6$ must be attributed to additional factors, such as the presence of the second COO^- group and/or the second hydration shell. As the XRD study reported the presence of the 13 water molecules in the channel, the effect of the second hydration shell should be considered. Indeed, for Mg^{2+} in water, *a priori* 6 water molecules form the first shell and the next 12 molecules the second one.[21] According to the Nureki's crystal structure, the second shell in the Mg^{2+} channel is filled by 7 water molecules and 4 oxygen atoms in the peptide framework, instead of 12 water molecules.

The effect of higher hydration can be explored by the infrared spectra in Fig. 3. The spectrum changes significantly when the 10th water molecule is added to the cluster (see Fig. 3 for the change from n = 9 to 10). In the δ^{CH} range at around 1430 cm^{-1}, the intensity of one band (green) is significantly enhanced. In contrast, ν_s^{coo-} becomes weaker. Such a clear spectral change reveals a notable modification of the hydration condition of the ($Mg^{2+}\cdots COO^-$) ion pair. This spectral feature keeps going up to n = 13, before another clear spectral change takes place at n = 14 where ν_s^{coo-} is no more observed, leaving onlyν^{co}-like bands. If we take the simple analogy of the calculated structures for n = 6, the disappearance of ν_s^{coo-} from n = 13 to n = 14 strongly suggests the complete transition from full-contact ion pairs to partially-separated or separated ones. Similarly, the spectral change from n = 9 to n = 10 suggests that $[CH_3COOMg]^+\cdot(H_2O)_{10-13}$ clusters are a mixture of full-contact ion pairs with partially-separated or separated ones.

These interpretations are further examined by more sophisticated simulations for two critical cluster sizes n = 10 and 14. By investigating a set of structures representative of the diversity encountered in these clusters, the simulated spectra enable us to study the influence of the partially-filled second hydration shell. These energy-weighted averaged spectra are presented in Fig. 4 (see ESI† for details). It should be noted that the labels of the vibrational bands in Fig. 2 and 3 are slightly different from Fig. 4 because the description of the vibrational motions in terms of internal coordinates changes with the size of the clusters. The former figures present calculated systems with only 6 water molecules, while the latter show an average of various conformations for n = 10 and 14 clusters. The correspondence between the assignments in Fig. 2 and 4 are explained in ESI.†

First, according to the theoretical spectra for n = 10 (Fig. 4a), the whole experimental spectrum is consistent with the coexistence of only two types of structures: (i) a full contact ion pair whose vibrational pattern can be continuously tracked from n = 4 (Fig. 3), the poor agreement near 1500 cm^{-1} only resulting from the insufficient description of the ν_s^{coo-} and δ^{CH_3} coupling[30] by harmonic frequency calculations. (ii) a partially separated ion pair, which is assigned to the new spectral features popping up at n = 10, *e.g.* the blue-most component of the ν_{as}^{coo-} band (blue band) and the main red-most feature (green band) in the ν_s^{coo-} spectral region. In addition, both these ion pairs are isoenergetic (ESI†), supporting their simultaneous observation at this cluster size. In turn, separated ion pairs present the worst ν_a^{coo-} frequency and energy agreement (ESI†). For n = 14, the specific signature of the full contact ion pair disappears (red band in Fig. 3 and 4), in agreement with

the significant increase in their relative energy compared to $n = 10$ (ESI†). In parallel, the triplet on the green band is most likely explained by the coexistence of several structures. According to calculated ν_{as}^{coo-} bands (Fig. 4b), partially separated ion pairs best agree with the experiment, suggesting that the IR spectrum results mainly from a mixture of several partially separated ion pairs. Alternatively, the appearance of separated ion pairs should be accompanied by a new red-shifted ν_{as}^{coo-} band, which is not observed. By comparing $n = 10$ and $n = 14$ spectra, however, a modest red-shift of ν_{as}^{coo-} (~ 3 cm^{-1}) is observed and could be interpreted as the manifestation of the presence of separated ion pairs as minor species.

4. Conclusions

$Mg^{2+}(H_2O)_6$ transportation through $RCOO^-$ ion selection filters in MgtE corresponds to the separation of $(RCOO^-)_2{\cdot}Mg^{2+}$ ion pairs by 6 water molecules if we focus on the local structure. From accumulated knowledge on ion pair solvation, we pointed out that contact ion pairs in the channel could compete with separated ion pairs. This hydration-induced separation of $RCOO^-\cdots Mg^{2+}$ and its dependence on the number of water molecules has been explored by cold ion trap IR laser spectroscopy in which the separation of the ion pair can be detected by the shift of IR frequencies for specific sizes of $[CH_3COOMg]^+(H_2O)_n$ (n = 4–17) clusters. With the help of quantum chemistry calculations, the shifts of the vibrational bands in the 1300–1800 cm^{-1} range were interpreted along this series. The nature of the ion pair, *i.e.* full contact, partially-separated and separated, is monitored by following the vibrational frequencies and intensities of the CO_2^- stretch marker bands. No clear change of these vibrational bands has been observed from n = 4 to 9, which demonstrates that the hydration by six water molecules cannot disturb the strong interaction $RCOO^-\cdots Mg^{2+}$. Consequently, additional factors other than these six water molecules have to be invoked to promote the transportation of Mg^{2+}. Note that the presence of another $RCOO^-$ does not explain the central transportation path between the pair of $RCOO^-$ automatically because two charge center produces the double minimum potential in which Mg^{2+} ion have to be located at one of $RCOO^-$, not at the center. The results suggest that the transportation of hexa-hydrated Mg^{2+} have to be rationalized not only by the interaction to the pair of $RCOO^-$ but also by the additional factors, such as the circulstance generated by other part of the channel and/or higher hydration. Considering additional water molecules in the second solvation shell of Mg^{2+}, the change of the marker bands revealed significant structural changes upon hydration from $n = 9$ to $n = 10$, and $n = 13$ to $n = 14$. From the more sophisticated quantum chemistry calculations, the former change in the vibrational spectrum is rationalized by the formation of partially-separated ion pairs, while the latter is consistent with the disappearance of the full contact ion pair and the dominant formation of several partially-separated ion pairs together with minor separated ion pairs. It may suggest that the transportation of Mg^{2+} in MgtE, where separated ion pairs are found in XRD of the crystal, may require hydration by at least 14 water molecules. In other sense, Mg^{2+} would be transported without help of the circulstance generated by the whole protein if Mg^{2+} is hydrated enough. Interestingly, the XRD analysis[21] of the channel shows 13 water molecules, which echo our conclusion. Overall, these results highlight the strength of our bottom-up approach using solvated ion pair clusters. They reveal the importance of various contributions of the molecular environment in Mg^{2+} transportation, which have not been discussed yet. The transportation of other divalent ions such as Ca^{2+} should also be studied with a similar approach in the future.

Author contributions

E. G., S. I. and M. F. designed the project. H. T., K. H. and S. I. conducted experiment with simple calculations, whereas J. X. B., V. B. and E. G. performed sophisticated level calculations. The manuscript was written through contributions of all authors. All authors have given approval to the final version of the manuscript.

Conflicts of interest

There are no conflicts to declare.

Acknowledgements

The authors are grateful to Dr Michel Mons for his interest in this study and his advice. This study has been made possible thanks to the following grants: KAKENHI (JP20H00372, JP20K20446, JP21H04674, JP21K14585) and the Core-to-core program (JPJSCCA20210004) of JSPS, World Research Hub Initiatives in Tokyo Institute of Technology, the Cooperative Research Program of the ''Network Joint Research Center for Materials and Devices'' from the Ministry of Education, Culture, Sports, Science and Technology (MEXT), Japan, and the RIKEN Pioneering Project, ''Fundamental Principles Underlying the Hierarchy of Matter: A Comprehensive Experimental Study''; ANR grants IONPAIRS ANR-16-CE29-0017 and VAPOBIO ANR-20-CE29-0016. The computations were in part performed at the Research Center for Computational Science, Okazaki, Japan (21-IMS-C109).

References

1 D. A. Doyle, J. M. Cabral, R. A. Pfuetzner, A. Kuo, J. M. Gulbis, S. L. Cohen, B. T. Chait and R. MacKinnon, *Science*, 1998, **280**, 69–77.
2 Y. Zhou, J. H. Morais-Cabral, A. Kaufman and R. MacKinnon, *Nature*, 2001, **414**, 43–48.
3 J. Payandeh, T. Scheuer, N. Zheng and W. A. Catterall, *Nature*, 2011, **475**, 353–358.

4 L. Tang, T. M. Gamal El-Din, J. Payandeh, G. Q. Martinez, T. M. Heard, T. Scheuer, N. Zheng and W. A. Catterall, *Nature*, 2014, **505**, 56–61.
5 H. T. Kratochvil, J. K. Carr, K. Matulef, A. W. Annen, H. Li, M. Maj, J. Ostmeyer, A. L. Serrano, H. Raghuraman and S. D. Moran, *et al.*, *Science*, 2016, **353**, 1040–1044.
6 S. Bernèche and B. Roux, *Biophys. J.*, 2000, **78**, 2900–2917.
7 D. A. Köpfer, C. Song, T. Gruene, G. M. Sheldrick, U. Zachariae and B. L. de Groot, *Science*, 2014, **346**, 352–355.
8 W. Kopec, D. A. Köpfer, O. N. Vickery, A. S. Bondarenko, T. L. C. Jansen, B. L. de Groot and U. Zachariae, *Nat. Chem.*, 2018, **10**, 813–820.
9 S. Ishiuchi, Y. Sasaki, J. M. Lisy and M. Fujii, *Phys. Chem. Chem. Phys.*, 2019, **21**, 561–571.
10 R. Otsuka, K. Hirata, Y. Sasaki, J. M. Lisy, S. Ishiuchi and M. Fujii, *Chem. Phys. Chem.*, 2020, **21**, 712–724.
11 T. Negoro, K. Hirata, J. M. Lisy, S. Ishiuchi and M. Fujii, *Phys. Chem. Chem. Phys.*, 2021, **23**, 12045–12050.
12 Y. Suzuki, K. Hirata, J. M. Lisy, S. Ishiuchi and M. Fujii, *J. Phys. Chem. A*, 2021, **125**, 9609–9618.
13 J. Payandeh and E. F. Pai, *EMBO J.*, 2006, **25**, 3762–3773.
14 S. Eshaghi, D. Niegowski, A. Kohl, D. M. Molina, S. A. Lesley and P. Nordlund, *Science*, 2006, **313**, 354–357.
15 V. V. Lunin, E. Dobrovetsky, G. Khutoreskaya, R. Zhang, A. Joachimiak, D. A. Doyle, A. Bochkarev, M. E. Maguire, A. M. Edwards and C. M. Koth, *Nature*, 2006, **440**, 833–837.
16 A. Guskov, N. Nordin, A. Reynaud, H. Engman, A.-K. Lundbäck, O. Jong Agnes Jin, T. Cornvik, T. Phua and S. Eshaghi, *Proc. Natl. Acad. Sci. U. S. A.*, 2012, **109**, 18459–18464.
17 Y. Huang, F. Jin, Y. Funato, Z. Xu, W. Zhu, J. Wang, M. Sun, Y. Zhao, Y. Yu and H. Miki, *et al.*, *Sci. Adv.*, 2021, **7**, eabe6140.
18 M. Konrad, K. P. Schlingmann and T. Gudermann, *Am. J. Phys. Renal. Phys.*, 2004, **286**, F599–F605.
19 M. Hattori, Y. Tanaka, S. Fukai, R. Ishitani and O. Nureki, *Nature*, 2007, **448**, 1072–1075.
20 M. Hattori, N. Iwase, N. Furuya, Y. Tanaka, T. Tsukazaki, R. Ishitani, M. E. Maguire, K. Ito, A. Maturana and O. Nureki, *EMBO J.*, 2009, **28**, 3602–3612.
21 H. Takeda, M. Hattori, T. Nishizawa, K. Yamashita, S. T. A. Shah, M. Caffrey, A. D. Maturana, R. Ishitani and O. Nureki, *Nat. Commun.*, 2014, **5**, 5374.
22 X. Teng, D. Sheng, J. Wang, Y. Yu and M. Hattori, *iScience*, 2022, **25**, 105565.
23 F. J. Martínez Casado, M. Ramos Riesco, M. I. Redondo, D. Choquesillo-Lazarte, S. López-Andrés and J. A. R. Cheda, *Cryst. Growth Des.*, 2011, **11**, 1021–1032.
24 J. Donon, S. Habka, T. Very, F. Charnay-Pouget, M. Mons, D. J. Aitken, V. Brenner and E. Gloaguen, *Chem. Phys. Chem.*, 2021, **22**, 2442–2455.
25 R.-Z. Li, C.-W. Liu, Y. Q. Gao, H. Jiang, H.-G. Xu and W.-J. Zheng, *J. Am. Chem. Soc.*, 2013, **135**, 5190–5199.
26 C. J. Johnson, L. C. Dzugan, A. B. Wolk, C. M. Leavitt, J. A. Fournier, A. B. McCoy and M. A. Johnson, *J. Phys. Chem. A*, 2014, **118**, 7590–7597.
27 W.-J. Zhang, G.-L. Hou, P. Wang, H.-G. Xu, G. Feng, X.-L. Xu and W.-J. Zheng, *J. Chem. Phys.*, 2015, **143**, 054302.
28 G.-L. Hou, C.-W. Liu, R.-Z. Li, H.-G. Xu, Y. Q. Gao and W.-J. Zheng, *J. Phys. Chem. Lett.*, 2017, **8**, 13–20.
29 A. M. Sadoon, G. Sarma, E. M. Cunningham, J. Tandy, M. W. D. Hanson-Heine, N. A. Besley, S. Yang and A. M. Ellis, *J. Phys. Chem. A*, 2016, **120**, 8085–8092.
30 J. W. DePalma, P. J. Kelleher, L. C. Tavares and M. A. Johnson, *J. Phys. Chem. Lett.*, 2017, **8**, 484–488.
31 J. K. Denton, P. J. Kelleher, M. A. Johnson, M. D. Baer, S. M. Kathmann, C. J. Mundy, R. B. A. Wellen, H. C. Allen, T. H. Choi and K. D. Jordan, *Proc. Natl. Acad. Sci. U. S. A.*, 2019, **116**, 14874–14880.
32 J. Donon, J.-X. Bardaud, V. Brenner, S. Ishiuchi, M. Fujii and E. Gloaguen, *Phys. Chem. Chem. Phys.*, 2022, **24**, 12121–12125.
33 A. Chakraborty, S. Schmahl and K. R. Asmis, *Chem. Phys. Chem.*, 2021, **22**, 1036–1041.
34 K. D. Collins, *Biophys. Chem.*, 2006, **119**, 271–281.
35 M. Z. Kamrath, E. Garand, P. A. Jordan, C. M. Leavitt, A. B. Wolk, M. J. Van Stipdonk, S. J. Miller and M. A. Johnson, *J. Am. Chem. Soc.*, 2011, **133**, 6440–6448.
36 N. S. Nagornova, T. R. Rizzo and O. V. Boyarkin, *Science*, 2012, **336**, 320–323.
37 J. Jašík, J. Žabka, J. Roithová and D. Gerlich, *Int. J. Mass Spectrom.*, 2013, **354–355**, 204–210.
38 Y. Inokuchi, K. Soga, K. Hirai, M. Kida, F. Morishima and T. Ebata, *J. Phys. Chem. A*, 2015, **119**, 8512–8518.
39 S. Ishiuchi, H. Wako, D. Kato and M. Fujii, *J. Mol. Spectrosc.*, 2017, **332**, 45–51.
40 B. M. Marsh, J. M. Voss and E. Garand, *J. Chem. Phys.*, 2015, **143**, 204201.
41 E. Sato, K. Hirata, J. M. Lisy, S. Ishiuchi and M. Fujii, *J. Phys. Chem. Lett.*, 2021, **12**, 1754–1758.
42 S. Grimme, J. Antony, S. Ehrlich and H. Krieg, *J. Chem. Phys.*, 2010, **132**, 154104.
43 T. Yanai, D. P. Tew and N. C. Handy, *Chem. Phys. Lett.*, 2004, **393**, 51–57.
44 R. Krishnan, J. S. Binkley, R. Seeger and J. A. Pople, *J. Chem. Phys.*, 2008, **72**, 650–654.
45 A. D. McLean and G. S. Chandler, *J. Chem. Phys.*, 2008, **72**, 5639–5648.
46 J. Paterová, J. Heyda, P. Jungwirth, C. J. Shaffer, Á. Révész, E. L. Zins and D. Schröder, *J. Phys. Chem. A*, 2011, **115**, 6813–6819.
47 E. Gloaguen, M. Mons, K. Schwing and M. Gerhards, *Chem. Rev.*, 2020, **120**, 12490–12562.
48 A. Schäfer, C. Huber and R. Ahlrichs, *J. Chem. Phys.*, 1994, **100**, 5829–5835.
49 F. Weigend, M. Häser, H. Patzelt and R. Ahlrichs, *Chem. Phys. Lett.*, 1998, **294**, 143–152.
50 R. Ahlrichs, M. Bär, M. Häser, H. Horn and C. Kölmel, *Chem. Phys. Lett.*, 1989, **162**, 165–169.
51 S. Habka, T. Very, J. Donon, V. Vaquero-Vara, B. Tardivel, F. Charnay-Pouget, M. Mons, D. J. Aitken, V. Brenner and E. Gloaguen, *Phys. Chem. Chem. Phys.*, 2019, **21**, 12798–12805.

